Advances in Geo-Energy Research

Vol. 13, No. 1, p. 32-41, 2024

Original article

A new pixel-free algorithm of pore-network extraction for fluid flow in porous media: Flashlight search medial axis

Jie Liu[1], Tao Zhang[1,2]*, Shuyu Sun[1]*

[1]*Physics Science and Engineering, King Abdullah University of Science and Technology, Thuwal 23955-6900, Saudi Arabia*

[2]*Institute of New Energy, China University of Petroleum (East China), Qingdao 266580, P. R. China*

Keywords:
Pore-network model
pore-network extraction
pixel-free
continuum extraction approach

Cited as:
Liu, J., Zhang, T., Sun, S. A new pixel-free algorithm of pore-network extraction for fluid flow in porous media: Flashlight search medial axis. Advances in Geo-Energy Research, 2024, 13(1): 32-41.
https://doi.org/10.46690/ager.2024.07.05

Abstract:
Pore-network models have become a critical tool in the study of fluid flow in geo-energy researches over the last few decades, and the accuracy of pore-network modeling results highly depends on the extraction of pore networks. Traditional methods of pore-network extraction are based on pixels and require images with high quality. Here, a pixel-free method called the flashlight search medial axis algorithm is proposed for pore-network extraction in a continuous space. The search domain in a two-dimensional space is a line, whereas a surface domain is searched in a three-dimensional scenario. Thus, the algorithm follows the dimensionality reduction idea; the medial axis can be identified using only a few points instead of calculating every point in the void space. In this way, computational complexity of this method is greatly reduced compared to that of traditional pixel-based extraction methods, thus enabling large-scale pore-network extraction. Based on cases featuring two- and three-dimensional porous media, the algorithm performs well regardless of the topological structure of the pore network or the positions of the pore and throat centers. This algorithm can also be used to examine both closed-boundary and open-boundary cases. Finally, this algorithm can identify the medial axis accurately, which is of great significance in the study of geo-energy.

1. Introduction

Porous media have been considered effective fluid carriers in various geo-energy fields in the last few decades, such as hydrogen and carbon dioxide storage (Makal et al., 2012; Heinemann et al., 2021), and digital rock study in reservoirs (Sun and Zhang, 2020; Shan et al., 2022b). Porous media have complex topological structures induced by various pores and throats (Dullien, 1975; Raoof and Hassanizadeh, 2010), thus, it is imperative that porous media should be accurately described to conduct further numerical investigation.

Porous media are commonly found in a wide range of areas, especially petroleum and natural gas reservoirs (Cao et al., 2020). Advancements in CT scanning have enabled the visualization of the inner void structures of rock matrixes (Mostaghimi et al., 2013; Song et al., 2021), which reveals complex topological structures comprising pores and throats. Problems in porous media have been studied using several numerical approaches, such as the lattice Boltzmann method (Zhang and Sun, 2019), phase field method (Zhu et al., 2020), and smoothed-particle hydrodynamics (Liu et al., 2022a; Feng et al., 2023). Molecular simulation methods have also been employed to reveal the micro-scale mechanisms (Yang et al., 2020; Liu et al., 2024), notably the fluid behavior in nanoscale pores (Liu et al., 2022b; Shan et al., 2022a). However, calculating single- or multi-phase flow in complex pore spaces is usually computationally challenging. Numerical discretization methods, such as finite volume and finite element methods, require the generation of highly accurate unstructured meshes for porous media (Javandel and Witherspoon, 1968; Yang et al., 2019). Therefore, a simplified numerical method is necessary to solve problems in complex porous media.

The first pore-network model (PNM) was proposed by Fatt (1956); a regular two-dimensional lattice was built using

*Corresponding author.
E-mail address: jie.liu.1@kasut.edu.sa (J. Liu); tao.zhang.1@kaust.edu.sa (T. Zhang); shuyu.sun@kaust.edu.sa (S. Sun).

Yandy Scientific Press

2207-9963
Received May 4, 2024; revised May 21, 2024; accepted June 8, 2024; available online June 11, 2024.

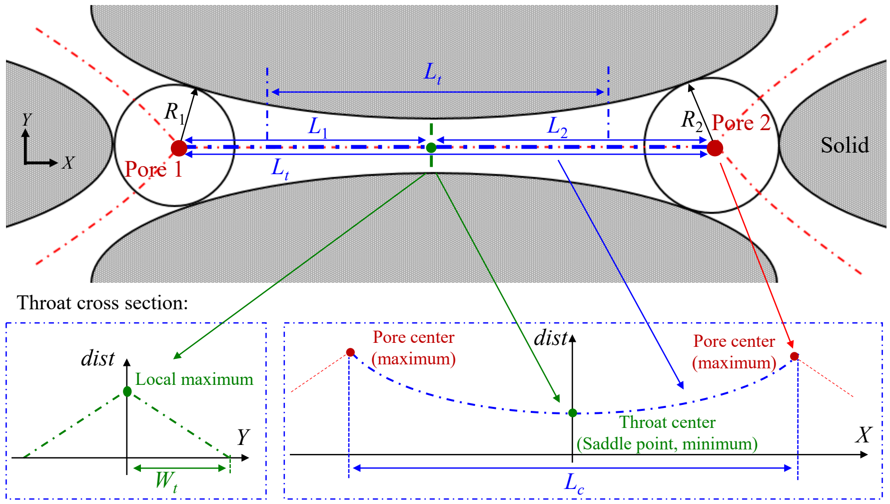

Fig. 1. Schematic of medial axis characteristics.

random radii to predict the capillary pressure and relative permeability. However, a regular pore network is not capable of representing the topology and geometry of porous media. Bryant and Blunt (1992) studied pore-network extraction from a realistic porous media, in which uniform spheres were packed, leading to the conclusion that the pores were packed in a tetrahedral configuration. Furthermore, they predicted the relative permeability of a sand pack, which agreed well with results for sandstone. The growth of PNMs has enabled them to overcome the problems associated with irregular lattices, varying wetting conditions, and multi-phase flow (Blunt et al., 2002; Balhoff and Wheeler, 2009; Ryazanov et al., 2009). This technique is also useful for handling more complex problems, such as non-Newtonian, non-Darcy, and reactive flows (Lopez et al., 2003; Yiotis et al., 2006). Song et al. (2023) proposed a general PNM based on three-phase thermodynamic equilibrium, and predicted multicomponent flow in nanoporous shale. The computational speed of PNMs is considerably faster than that of mesh-based methods; however, their accuracy relies on pore-network extraction.

The medial axis and maximal ball methods are commonly used to extract the pore networks of porous media (Bultreys et al., 2020; Cui et al., 2022). Based on the inherent porous characteristics of a porous medium, the medial axis is situated in the middle of the geometric pore space (Blunt, 2001). A significant advantage of the medial axis method is its capacity to reduce dimensionality. For instance, in the case of the two-dimensional domain, the medial axis is comprised of medial lines, while in the case of the three-dimensional domain, the medial axis is comprised of the intersection of several medial surfaces. Burning algorithms are commonly used to determine the medial pixel or voxel in the medial axis method. This process involves burning the cells from the solid phase to the void phase one layer at a time (Xiong et al., 2016). In the maximal ball method (Dong and Blunt, 2009), the largest inscribed balls are searched in the void space, and balls contained within other balls are removed. The maximal balls are used to identify pores, and the smallest balls are used to identify throats. However, in both the medial axis and maximal ball algorithms, extraction relies on image quality, which is typically based on the resolution. Thus, a single extraction algorithm may yield varying results when subjected to varying resolutions.

In this study, the flashlight search medial axis (FSMA) algorithm, a pixel-free pore-network extraction algorithm for continuous spaces, was proposed. Theoretically, the FSMA algorithm has a high pore-network extraction efficiency, as dimensionality-reduced search is performed in a two-dimensional or three-dimensional space, where only a small part of the data are used to identify the medial axis.

2. Methodology

2.1 Characteristics of medial axis

The minimum distance between a random point in the void space and a point in the solid phase is determined as follows:

$$dist(x,D) = \min\{dist(x,y), y \in D\} \tag{1}$$

where D represents the solid phase, y represents the point in the solid phase, x represents the point in the void phase, and *dist* represents the minimum distance. In an image, a pixel of a solid phase can be visualized and considered a point in that solid phase. The distance map is obtained using the above equation. As shown in Fig. 1, the *dist* of the pore center is the maximum in that pore space, which is similar to the mountain top. The points on the medial axis are local maxima; the gradient of *dist* is discontinued, and the curve resembles a mountain ridge. One special point is the throat center, where *dist* is the minimum along the medial axis. The throat center is also a saddle point; the minimum and local maximum are in the direction of the medial axis and the direction perpendicular to the medial axis, respectively. The medial axis comprises the discontinuation points of *dist*'s gradient, which are called critical points, suggesting that the medial axis can be determined accordingly. As depicted in Fig. 1, the total length between two pores is defined as the

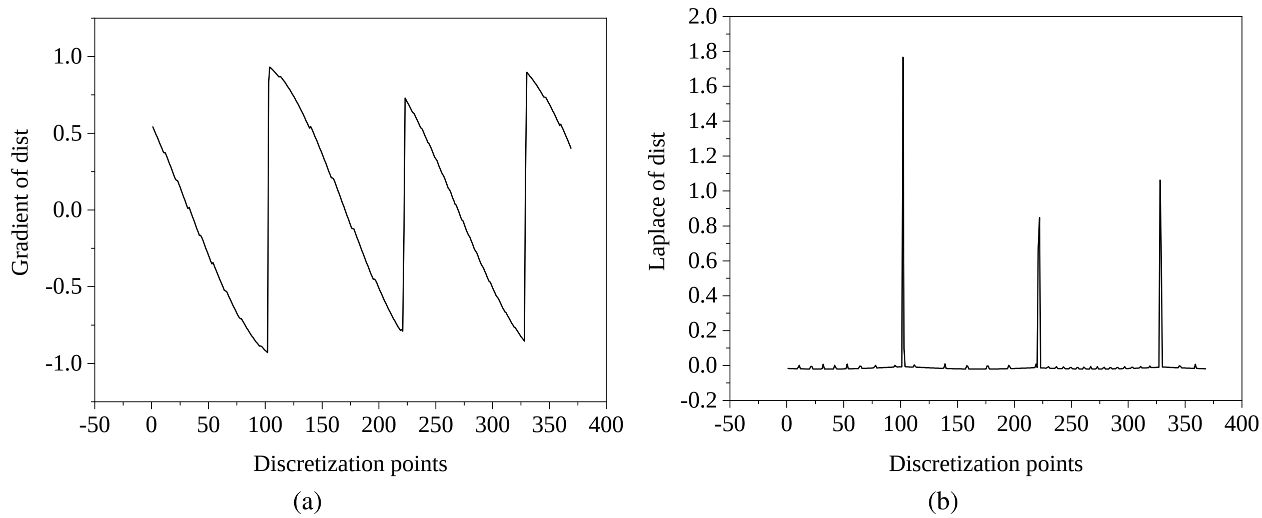

Fig. 2. (a) Gradient of *dist* and (b) Laplace of *dist*.

summation of two parts of lengths from the pore center to the throat center, which can be expressed as follows:

$$L_c = L_1 + L_2 \tag{2}$$

where L_c is the length between the two pore centers, L_1 and L_2 represent the lengths between the pore centers and the throat center. If the inscribed sphere is considered the pore body, then the following equation is the simplest way to determine the length of the throat channel:

$$L_t = L_1 - R_1 + L_2 - R_2 \tag{3}$$

where L_t is the length of the throat channel, R_1 and R_2 are the radii of two inscribed spheres. However, the volume of the pore body is larger than the volume occupied by the inscribed sphere. The length fraction between the pore body and the throat channel is handled as follows:

$$L_t = L_1 - \alpha\frac{L_1 W_t}{R_1} + L_2 - \alpha\frac{L_2 W_t}{R_2} \tag{4}$$

where W_t is the *dist* value at the throat center and α is the pore-throat segmentation coefficient. In this regard, the segment coefficient is usually set to 0.5 or 0.6 in previous studies (Øren and Bakke, 2003; Dong and Blunt, 2009).

2.2 FSMA pore-network extraction algorithm

2.2.1 Two-dimensional pore-network extraction algorithm

Based on the properties presented in Section 2.1, two-dimensional pore-network extraction is completed as follows:

Step 1: Determine the pore center from a random point in the void space using the steepest-descent method. The calculation domain for the initial point is discretized in the form of a circle to search for the maximum descent. The search range should be as short as possible to ensure the accuracy of pore-center calculation. In our experience, this range should be equivalent to the size of a pixel. Thus, the point is updated with the search step size of the range until the pore center is reached. This process can be likened to a person climbing the steepest route to reach a mountain's summit.

Step 2: From the first pore center, find the medial axis directions. On the position of pore center, the $dist(x,D)$ is maximum, so there are some critical points lie around the pore center. Circle discretization is applied around the pore center. The medial axis can be determined via a critical point. As seen in Fig. 2, in a case involving three medial axes from one pore center, three critical points are determined using the gradient and Laplace of *dist*.

Step 3: Flashlight searching method to update the critical point on the medial axis. Once the direction of the medial axis is determined, a fan-shaped region is adopted to search for the next critical point. The radio of the fan-shaped region should be smaller than the radio of the circular search region. The critical point can be updated along the medial axis by following this rule. As shown in Fig. 3, the medial axis (*ma*) is determined one step at a time, and the critical point (*cp*) at each step is searched by building a fan-shaped region with a radius of r_s. Thus, the total length between two pores (pc_1 and pc_2) is expressed as follows:

$$L_t = L_1 + L_2 = \sum_{1}^{n_1} r_{si} + \sum_{n_1+1}^{n_2} r_{si} \tag{5}$$

where r_{si} is the search radius at step i, n_1 is the step number from the initial pore center to the throat center, and n_2 is the step number from the throat center to the next pore center.

Step 4: Judge the next pore center and throat center. The critical point is updated via the FSMA method. If the *dist* on the critical point reaches its maximum value, then that critical point is the pore center. If the *dist* on the critical point reaches its minimum value, then that critical point is the throat center.

Step 5: Exclude the overlapped pore centers. Since the medial axis will be determined from one pore center to another pore center, there will be some overlapped pore centers. Thus the overlapped pore centers need to be excluded to avoid repetitive calculations.

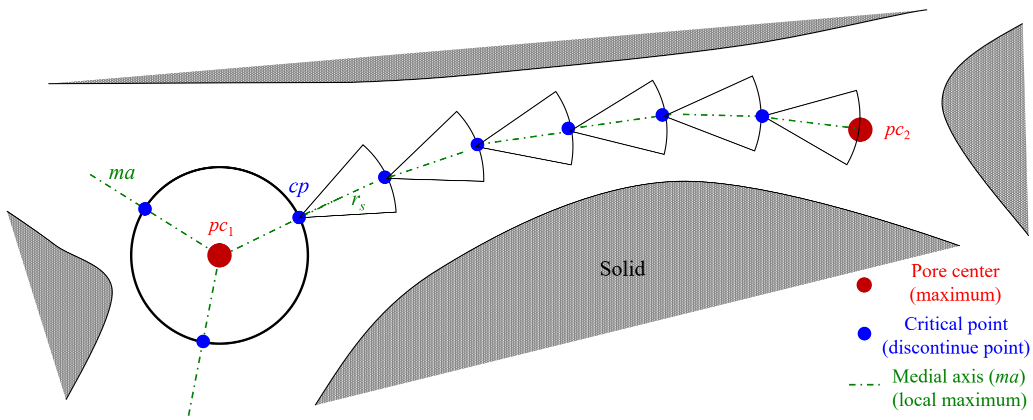

Fig. 3. Schematic of two-dimensional flashlight search.

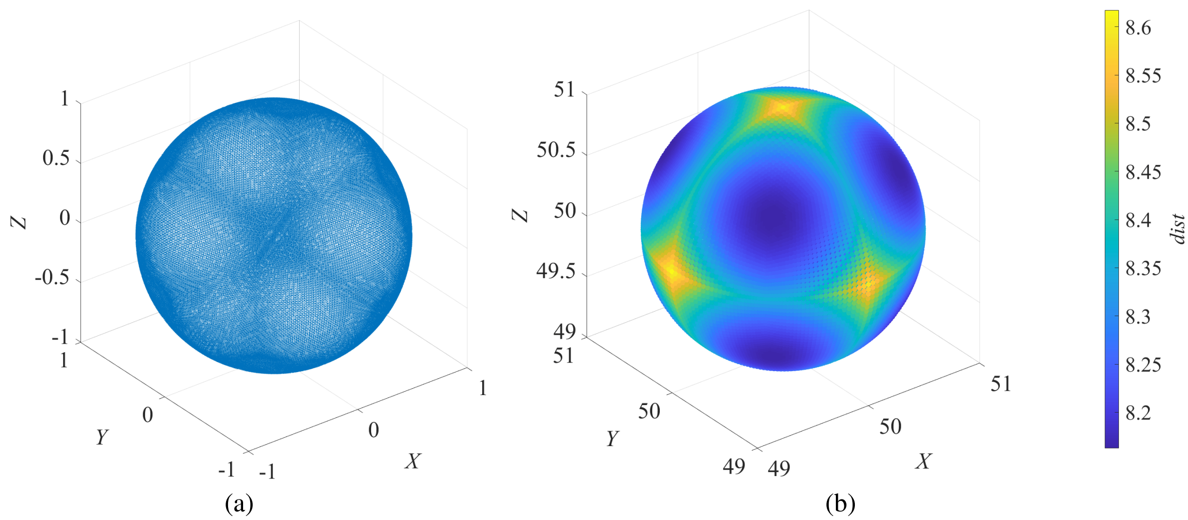

Fig. 4. Uniform sphere-packing scenario: (a) Projection from cube to sphere and (b) dist map on sphere surface.

2.2.2 Three-dimensional pore-network extraction algorithm

The idea underlying three-dimensional pore-network extraction is similar to the above, but the three-dimensional space introduces greater complexity.

Step 1: Find a pore center in the three-dimensional void space by using the steepest-descent method. Unlike the circular search region in the two-dimensional case, a spherical search region is adopted in the three-dimensional study, as seen in Fig. 4(a). The rest of the settings are the same as those in the two-dimensional case.

Step 2: Find the medial axis directions from the first pore center. Three-dimensional discretization is conducted, with the pore center regarded as the sphere center; this is achieved via projection from a cube to a sphere, as shown in Fig. 4(a). The *dist* map on the sphere surface can then be calculated, as seen in Fig. 4(b). Hence, discretization performs better in terms of mesh homogeneity. In Fig. 4, six local maximum points are observed on the sphere surface, which indicates the presence of six medial axis directions. The cross point of the medial surfaces is the medial axis point, suggesting that several medial surfaces form the medial axis.

Compared with classical (spherical-coordinate) discretization, the projection from the cube to the sphere has better discretization performance. The *dist* results of both discretization approaches along the medial axis are shown in Fig. 5. Misidentification may occur in Fig. 5(a), as the rough curve may induce some local minimum values along the medial axis. In Fig. 5(b), the *dist* shows a smoother curve, which is better for identifying the pore and throat centers.

Step 3: Update the critical points on the medial axis via the FSMA algorithm. Unlike the fan-shaped search region in the two-dimensional space, a cone-shaped search region is used in the three-dimensional space. The rest of the settings are the same as those in the two-dimensional case. In this manner, the critical points on the medial axis are determined by identifying the medial surfaces, as shown in Fig. 6.

Step 4: Judge the next pore center and throat centers. In the cone-shaped search region, the medial surface is reduced to a medial axis. Thus, the pore center in the cone-shaped search region is the cross point of several medial axes; the pore center has the maximum *dist* value. Along the medial axis, composed of the critical points, the throat center can be

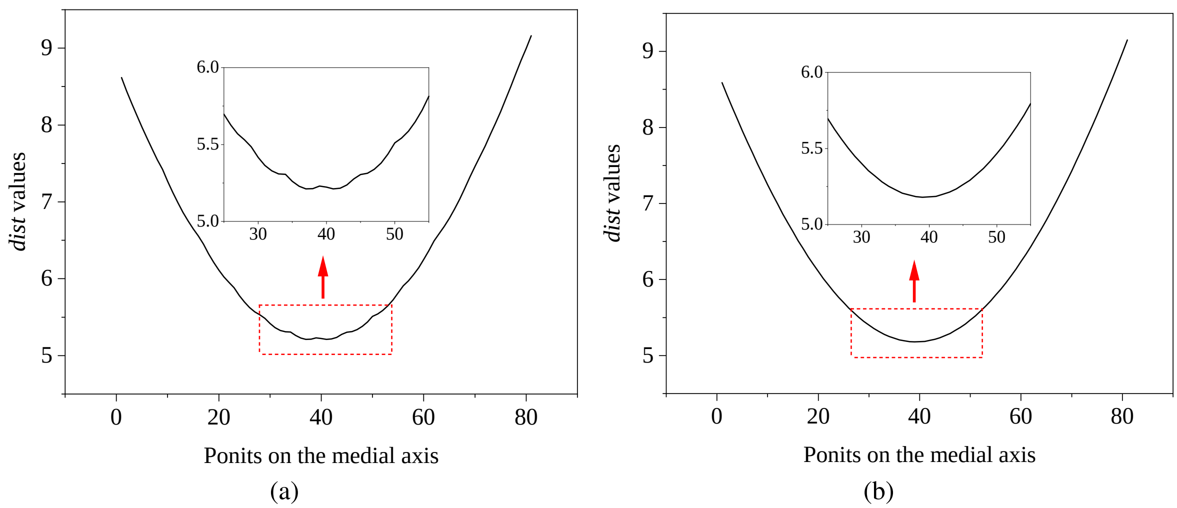

Fig. 5. *dist* values on medial axis obtained via (a) discretization using spherical coordinates and (b) discretization using cubic projection on sphere surface.

Algorithm 1: FSMA

```
Input  : A random initial point in the void space p;
         the known solid-phase data s; the search
         radius r_s to determine the critical point cp.
Output: The pore center pc; the medial axis ma;
         // According to Input
1  Find the first pore center p_1 using the steepest-descent
     method;
2  for search pore = 1 : m
   // From new-reached pore centers to
        further-reached pore centers
3  do
4  |  for search step = 1 : n
   |  // For the calculation of one strip
   |       of medial axis
5  |   do
6  |   |  Discretize the search region;
7  |   |  Determine the neighboring solid data from the
   |   |   previous cp;
8  |   |  Calculate the dist value of discretized points;
9  |   |  Judge the critical point;
   |   |  // Introduced in Output and Step
   |   |     1
10 |   |  if critical point cp_i reaches the pore center
   |   |  // Judge the pore center, in
   |   |     Step 2
11 |   |   then
12 |   |   |  pc_i = cp_i;
13 |   |   |  ma_i = {cp_1, ···, cp_i};
14 |   |  end
15 |  end
16 |  Update the new-searched pore centers;
17 |  Exclude overlapped pore centers;
   |  // According to Step 4
18 end
```

identified at the minimum of *dist*.

Table 1. Computational complexity of FSMA algorithm.

Line	Complexity	Description
Line 1	$O(s^2)$	Steepest-descent algorithm
Lines 6-9	$O(n\log n)$	Search for critical points
Lines 10-14	$O(k\times n)$	Determination of pore and throat centers
Lines 16-17	$O(n)$	Updating of pore and throat centers
Lines 1-18	$O(m\times(n\log n+k\times n+n))$	
Total	$O\left(s^2+m\times(n\log n+k\times n+n)\right)=O(mn\log n)$	

Step 5: Exclude the overlapped pore centers. This step is the same as the operation in the two-dimensional scenario.

The pseudocode of the FSMA algorithm is summarized as follows:

2.3 Comparative analysis of FSMA and pixel-based algorithms

Regarding to the traditional pore-network extraction methods, such as the maximal ball algorithm, the shape of the inscribed sphere highly depends on the image resolution. If the inscribed sphere is built on a low-resolution image, the boundary information of the inscribed sphere cannot be accurately described, and high-resolution images are computationally expensive. Therefore, the ability of the FSMA, a pixel-free method, to identify the medial axis regardless of image resolution is a natural advantage. Because of the dimensionality reduction idea during the search, computational complexity is reduced compared with that of traditional methods. The computational complexity of the FSMA algorithm is summarized in Table 1. As the steepest-descent method is only used once (for determining the first pore center), its complexity is not considered in the total code. k is the comparison number for the pore and throat centers; this value is usually too small

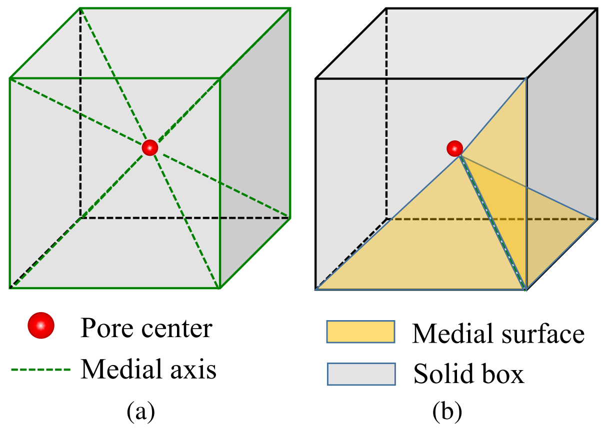

Fig. 6. Schematic of determination of medial axes: (a) Eight medial axes from pore center in cubic solid box and (b) one medial axis formed by three medial surfaces.

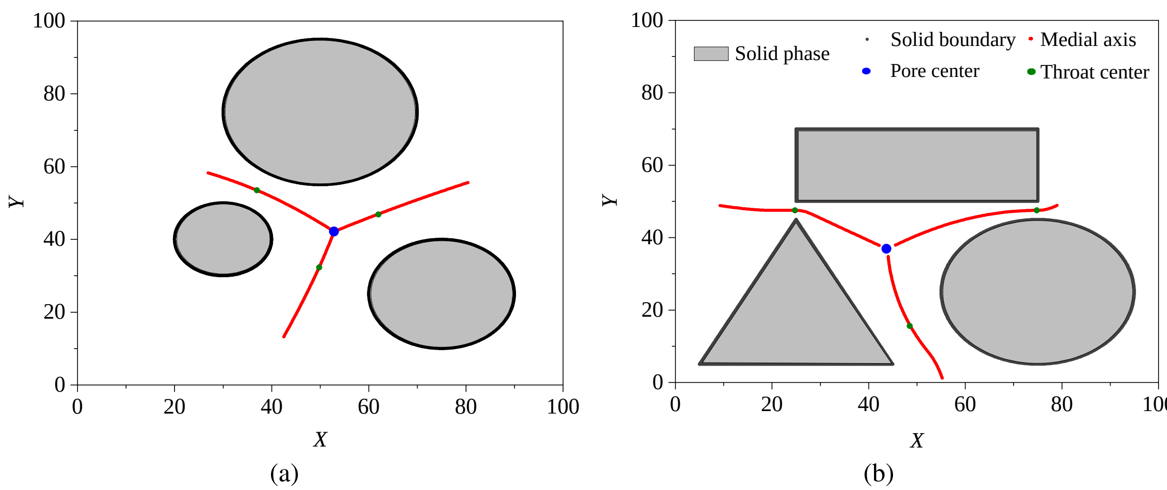

Fig. 7. Pore-network extraction in two-dimensional scenarios constructed using (a) spheres and (b) different shapes.

to add to the computational complexity.

The computational complexity of traditional pore-network extraction methods is expressed as follows:

$$O=(M+N)\left(\frac{L}{\varepsilon}\right)^{d} \tag{6}$$

where O represents the computational complexity; M and N are the numbers of pore and throat centers; d represents the dimensionality; L represents the size of the computational domain; and ε is the discretized unit, which is the size of the pixel or voxel in an image. Hence, L/ε is the number of points that should be calculated. The computational complexity of the FSMA algorithm is expressed as follows:

$$O=(M+N)\log\left(\frac{L}{\varepsilon}\right) \tag{7}$$

In a case where $L/\varepsilon=10$ in a three-dimensional space, the complexity of the FSMA algorithm is 1,000 times lower than that of traditional methods, in which all points need to be considered for one-time calculation.

3. Validation and discussions

3.1 Pore-network extraction from two-dimensional porous media

Although two-dimensional porous media have few application scenarios, such as artificial micro-fluidic chips, they should still be used for validation. A two-dimensional porous medium is built in a domain sized 100×100. The solid-phase regions are closed using known boundary points, suggesting that the *dist* value in the void phase can be calculated from these solid boundary points. The inner points in the solid phase are unnecessary, which helps save computer memory.

The medial axis starting from the first pore center is identified, as depicted in Fig. 7, which verifies the validity of the FSMA algorithm for the two-dimensional porous medium. On the medial axes, the throat centers can be determined accordingly; in addition, the throat centers are located at the positions of the minimum distance between two spheres, as shown in Fig. 7(a), which enables a clear assessment of the throat center calculation. In Fig. 7(b), the medial axis and th-

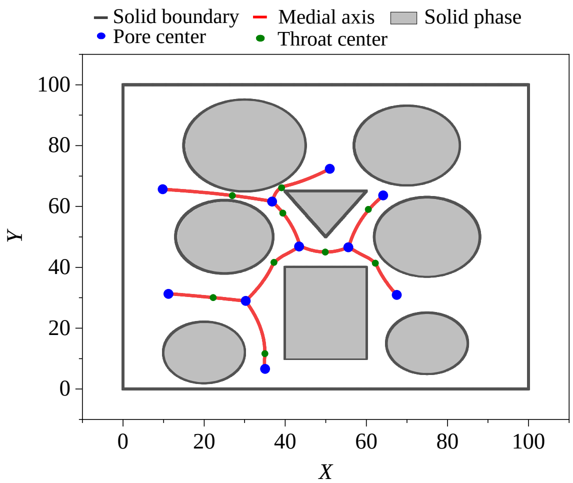

Fig. 8. Pore-network extraction from one pore center to other pore centers.

roat center can also be identified, suggesting that the FSMA algorithm can search the medial axis from one pore center via the dimensionality-reduced search method.

Once the medial axis is determined, the other pore centers can be searched from the first pore center and its medial axes. As shown in Fig. 8, the pore centers and medial axes comprise the topological structure of the porous medium. The pore network is identified gradually, pore center by pore center. Moreover, neighbor search is adopted in the search process. The *dist* values of the discretized points in the fan-shaped search region are calculated within the neighbor range, which is identified from the critical point in the previous step. Therefore, the pore-network construction of the FSMA algorithm only needs a small part of the information in the porous medium.

3.2 Boundary treatment

Boundary treatment is critical for pore-network extraction, as PNMs are used for fluid-flow simulation, which is a major application field in petroleum engineering (Golparvar et al., 2018; Zhao et al., 2023). Inflow and outflow boundaries are necessary for fluid-flow simulation, and dead-end corners are also considered as special boundaries in porous media (Lindquist and Venkatarangan, 1999; Yuan et al., 2022). The FSMA algorithm has a natural advantage in searching dead-end corners. As the FSMA algorithm is developed by searching medial axes for critical points, a critical point cannot be found in a dead-end corner within a search region. Therefore, dead-end corners are determined, as shown in Fig. 9. Despite the increase in the number of pore centers, the dead-end pore center can be ignored in some scenarios, such as single-phase fluid flow. However, in multi-phase fluid-flow problems, dead-end corners play an important role. Fluids with similar wettability to the rock surface are trapped in these corners, thus affecting the subsequent fluid flow.

Solid boundaries are a common boundary type in fluid-flow simulation, as the connectivity of pores and throats cannot be confirmed in porous media. In a solid boundary, the surface of a solid phase and a solid box form new pore channels. Dead-end corners are also generated in closed solid boxes, and they can be extracted when necessary. As seen in Fig. 10(a), the FSMA algorithm can search all critical points and extract the pore network in solid-box domains; this ability is meaningful in the study of reservoir rocks which have bad connectivity.

Open boundaries are also examined using the FSMA algorithm. In cases with open boundaries, the search operation proceeds until the boundary of the computational domain. The pore-network extraction is addressed in a domain where the right and left sides have open boundaries and the pore centers stop at the boundaries, as shown in Fig. 10(b); these are set as the Dirichlet boundary condition and the Neumann boundary condition, respectively (Raeini et al., 2012; Liu et al., 2020), and the fluid flow can be realized consequently.

3.3 Different packing styles for three-dimensional space

As shown in Fig. 11, a sphere-packing model is built in a cubic box sized $100 \times 100 \times$ to verify the FSMA algorithm in a three-dimensional space. Sixty-four solid spheres are packed in this box in a $4 \times 4 \times 4$ packing style The radius of each sphere is 12.5, suggesting that the spheres are in contact with each other. The surface of a solid sphere is discretized through regular hexahedron projection for better computational performance. The critical points are searched and the medial axis is identified in the three-dimensional space using the computational algorithm described in Section 2.2.2.

A regular packing style is adopted because the medial axis is connected as a regular network and is easily verified.

The beginning state of the medial axis was identified in Fig. 11(a), which is from the first pore center to a neighbor pore center through the connection of the medial axis. As seen in Fig. 11(b), the regular topological structure of the pore network is then extracted, revealing that the FSMA algorithm is applicable to three-dimensional porous media. Apart from the regular model, as depicted in Fig. 12, an irregular sphere-packing model is used to test the feasibility of the FSMA algorithm in a more complex porous medium, and it performs well.

4. Conclusions

In this study, a pore-network extraction algorithm called FSMA is proposed. The FSMA algorithm is developed in a continuous space rather than a pixel-based space, which makes it a pixel-free method. This algorithm adopts the idea of dimensionality-reduced search, making it unnecessary to calculate the global data for each pixel point. Thus, the algorithm has a substantially shorter computational time than traditional methods. In traditional search procedures, each point is calculated in the void space, whereas in the FSMA search procedure, only a few points need to be considered. In addition, the computation is further accelerated using neighbor search. Theoretically, the FSMA algorithm extracts pore networks with low computational complexity and high efficiency. These features are highly advantageous in large-scale pore-network extraction, and this algorithm enables the characterization of the PNM of a reservoir with a representative

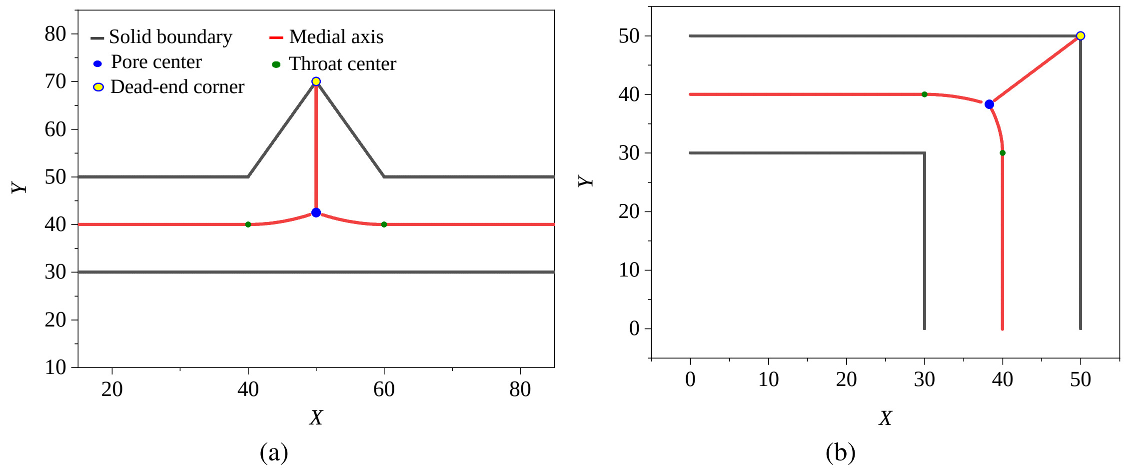

Fig. 9. Test cases of (a) a straight tube and (b) a elbow tube for FSMA algorithm featuring dead-end corners.

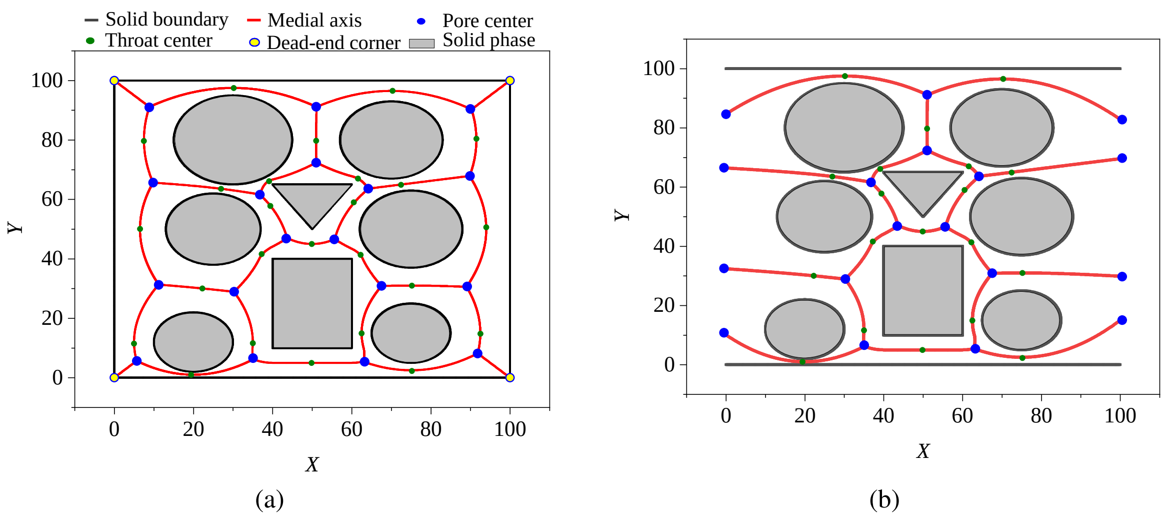

Fig. 10. Pore-network extraction within (a) closed (solid) and (b) open boundaries.

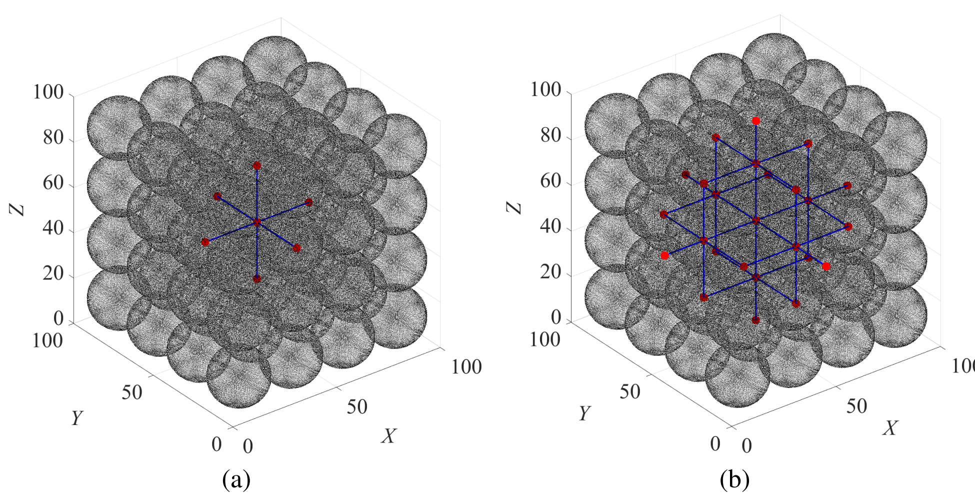

Fig. 11. Three-dimensional regular sphere-packing model and extracted medial axes: (a) beginning state and (b) extended state. Blue line represents the medial axis, and red point represents the pore center.

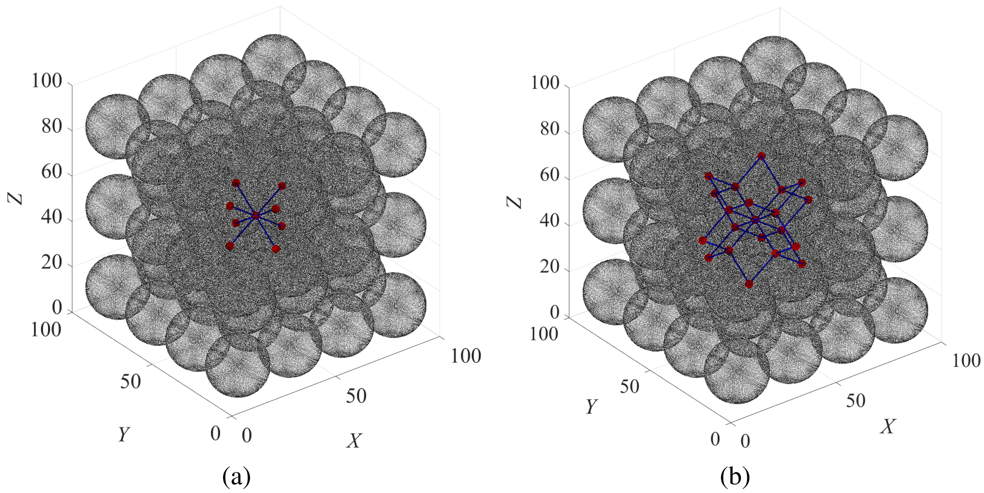

Fig. 12. Three-dimensional irregular sphere-packing model and extracted medial axis: (a) beginning state and (b) extended state. Blue line represents the medial axis, and red point represents the pore center.

elementary volume.

Specific computational programs are introduced for two- and three-dimensional spaces, and cases involving two- and three-dimensional porous media are constructed to verify the feasibility of the FSMA algorithm. The results indicate that the topological structure of the pore network is identified and the pore and throat centers are determined accordingly. Furthermore, according to a discussion of the boundary condition for the FSMA algorithm, the algorithm has the natural advantage of being able to search dead-end corners in porous media. Dead-end pore centers are identified by changing the determination conditions of the algorithm for searching critical points, which could be useful for studying multi-phase flow. Additionally, the algorithm performs well in both closed- and open-boundary tests. In conclusion, the pixel-free pore-network extraction algorithm FSMA can extract pore networks at high theoretical computational speeds and therefore has considerable potential for addressing large-scale geo-energy problems.

Acknowledgements

Thanks for the comments from each expert in the first “Geo-Energy Frontier Forum”. We would like to express appreciation to the following financial support: National Natural Scientific Foundation of China (No. 51936001), King Abdullah University of Science and Technology (KAUST) through the grants BAS/1/1351-01 and URF/1/5028-01. For computer time, this research used the resources of the Supercomputing Laboratory at King Abdullah University of Science & Technology (KAUST) in Thuwal, Saudi Arabia.

Conflict of interest

The authors declare no competing interest.

References

Balhoff, M. T., Wheeler, M. F. A predictive pore-scale model for non-darcy flow in porous media. SPE Journal, 2009, 14(4): 579-587.

Blunt, M. J. Flow in porous media—pore-network models and multiphase flow. Current Opinion in Colloid & Interface Science, 2001, 6(3): 197-207.

Blunt, M. J., Jackson, M. D., Piri, M., et al. Detailed physics, predictive capabilities and macroscopic consequences for pore-network models of multiphase flow. Advances in Water Resources, 2002, 25(8-12): 1069-1089.

Bryant, S., Blunt, M. Prediction of relative permeability in simple porous media. Physical Review A, 1992, 46(4): 2004.

Bultreys, T., Singh, K., Raeini, A. Q., et al. Verifying pore network models of imbibition in rocks using time-resolved synchrotron imaging. Water Resources Research, 2020, 56(6): e2019WR026587.

Cao, Y., Tang, M., Zhang, Q., et al. Dynamic capillary pressure analysis of tight sandstone based on digital rock model. Capillarity, 2020, 3(2): 28-35.

Cui, R., Hassanizadeh, S. M., Sun, S. Pore-network modeling of flow in shale nanopores: Network structure, flow principles, and computational algorithms. Earth-Science Reviews, 2022, 234: 104203.

Dong, H., Blunt, M. J. Pore-network extraction from micro-computerized-tomography images. Physical Review E, 2009, 80(3): 036307.

Dullien, F. Single phase flow through porous media and pore structure. The Chemical Engineering Journal, 1975, 10(1): 1-34.

Fatt, I. The network model of porous media. Transactions of the AIME, 1956, 207(1): 144-181.

Feng, X., Qiao, Z., Sun, S., et al. An energy-stable smoothed particle hydrodynamics discretization of the navier-stokes-cahn-hilliard model for incompressible two-phase flows. Journal of Computational Physics, 2023, 479:

111997.
Golparvar, A., Zhou, Y., Wu, K., et al. A comprehensive review of pore scale modeling methodologies for multiphase flow in porous media. Advances in Geo-Energy Research, 2018, 2(4): 418-440.
Heinemann, N., Alcalde, J., Miocic, J. M., et al. Enabling large-scale hydrogen storage in porous media-the scientific challenges. Energy & Environmental Science, 2021, 14(2): 853-864.
Javandel, I., Witherspoon, P. Application of the finite element method to transient flow in porous media. Society of Petroleum Engineers Journal, 1968, 8(3): 241-252.
Lindquist, W., Venkatarangan, A. Investigating 3D geometry of porous media from high resolution images. Physics and Chemistry of the Earth, Part A: Solid Earth and Geodesy, 1999, 24(7): 593-599.
Liu, C., Frank, F., Thiele, C., et al. An efficient numerical algorithm for solving viscosity contrast cahn-hilliard-navier-stokes system in porous media. Journal of Computational Physics, 2020, 400: 108948.
Liu, J., Xie, X., Meng, Q., et al. Effects of membrane structure on oil-water separation by smoothed particle hydrodynamics. Membranes, 2022a, 12(4): 387.
Liu, J., Zhang, T., Sun, S. Stability analysis of the water bridge in organic shale nanopores: A molecular dynamic study. Capillarity, 2022b, 5(4): 75-82.
Liu, J., Zhang, T., Sun, S. Molecular mechanisms of hydrogen leakage through caprock in moisture and residual gas conditions: A molecular dynamics-monte carlo study. Physics of Fluids, 2024, 36(2): 268169092.
Lopez, X., Valvatne, P. H., Blunt, M. J. Predictive network modeling of single-phase non-newtonian flow in porous media. Journal of Colloid and Interface Science, 2003, 264(1): 256-265.
Makal, T. A., Li, J. R., Lu, W., et al. Methane storage in advanced porous materials. Chemical Society Reviews, 2012, 41(23): 7761-7779.
Mostaghimi, P., Blunt, M. J., Bijeljic, B. Computations of absolute permeability on micro-ct images. Mathematical Geosciences, 2013, 45: 103-125.
Øren, P. E., Bakke, S. Reconstruction of berea sandstone and pore-scale modelling of wettability effects. Journal of Petroleum Science and Engineering, 2003, 39(3-4): 177-199.
Raeini, A. Q., Blunt, M. J., Bijeljic, B. Modelling two-phase flow in porous media at the pore scale using the volume-of-fluid method. Journal of Computational Physics, 2012, 231(17): 5653-5668.
Raoof, A., Hassanizadeh, S. M. A new method for generating pore-network models of porous media. Transport in Porous Media, 2010, 81: 391-407.
Ryazanov, A. V., Van Dijke, M. I. J., Sorbie, K. S. Two-phase pore-network modelling: Existence of oil layers during water invasion. Transport in Porous Media, 2009, 80: 79-99.
Shan, B., Ju, L., Guo, Z., et al. Investigation of shale gas flows under confinement using a self-consistent multiscale approach. Advances in Geo-Energy Research, 2022a, 6(6): 537-538.
Shan, L., Bai, X., Liu, C., et al. Super-resolution reconstruction of digital rock ct images based on residual attention mechanism. Advances in Geo-Energy Research, 2022b, 6(2): 157-168.
Song, R., Sun, S., Liu, J., et al. Pore scale modeling on dissociation and transportation of methane hydrate in porous sediments. Energy, 2021, 237: 121630.
Song, W., Yao, B., Sun, H., et al. Nanoscale three-phase transport in a shale pore network with phase change and solid-fluid interaction. Energy & Fuels, 2023, 37(18): 13851-13865.
Sun, S., Zhang, T. Reservoir Simulations: Machine Learning and Modeling. Texas, USA, Gulf Professional Publishing, 2020.
Xiong, Q., Baychev, T. G., Jivkov, A. P. Review of pore network modelling of porous media: Experimental characterisations, network constructions and applications to reactive transport. Journal of Contaminant Hydrology, 2016, 192: 101-117.
Yang, H., Sun, S., Li, Y., et al. A fully implicit constraint-preserving simulator for the black oil model of petroleum reservoirs. Journal of Computational Physics, 2019, 396: 347-363.
Yang, Y., Liu, J., Yao, J., et al. Adsorption behaviors of shale oil in kerogen slit by molecular simulation. Chemical Engineering Journal, 2020, 387: 124054.
Yiotis, A. G., Tsimpanogiannis, I. N., Stubos, A. K., et al. Pore-network study of the characteristic periods in the drying of porous materials. Journal of Colloid and Interface Science, 2006, 297(2): 738-748.
Yuan, Q., Ling, B., Aryana, S. A. New phase diagram of miscible viscous fingering instabilities in porous media with dead-end pores. Physics of Fluids, 2022, 34(9): 092109.
Zhang, T., Sun, S. A coupled lattice boltzmann approach to simulate gas flow and transport in shale reservoirs with dynamic sorption. Fuel, 2019, 246: 196-203.
Zhao, J., Liu, Y., Qin, F., et al. Pore-scale fluid flow simulation coupling lattice boltzmann method and pore network model. Capillarity, 2023, 7(3): 41-46.
Zhu, G., Kou, J., Yao, J., et al. A phase-field moving contact line model with soluble surfactants. Journal of Computational Physics, 2020, 405: 109170.